AGU Word Manuscript Template

STRESSES INDUCED BY MAGMA CHAMBER INFLATION ALTERED BY MECHANICAL LAYERING AND LAYER DIP

M. Clunes[1], J. Browning[1, 2], Jorge Cortez[1,3], José Cembrano[1], Carlos Marquardt[1, 2], Janine Kavanagh[4] and Agust Gudmundsson[5]

[1]Department of Structural and Geotechnical Engineering, Pontificia Universidad Católica de Chile, Santiago, Chile.
[2]Department of Mining Engineering, Pontificia Universidad Católica de Chile, Santiago, Chile.
[3]Department of Mining Engineering, Universidad de La Serena, La Serena, Chile.
[4]School of Environmental Sciences, University of Liverpool, Liverpool, United Kingdom
[5]Royal Holloway University of London, Department of Earth Sciences, Egham, United Kingdom

Corresponding author: Matías Clunes (mclunes@uc.cl)

Key Points:

- FEM models used to quantify the influence of layer dip on crustal stresses resulting from magma chamber inflation.
- Peak surface tensile stresses can shift by as much as 2 km, and can double in some cases, compared with elastic homogeneous assumptions.
- The effect is more pronounced with an idealized circular chamber when compared to a sill-like chamber.

Abstract

Understanding the stress distribution around shallow magma chambers is vital for predicting eruption sites and magma propagation directions. To achieve accurate predictions, comprehensive insight into the stress field surrounding magma chambers and near the surface is essential. Existing stress models for magma chamber inflation often assume a homogenous elastic half-space or a heterogeneous crust with varying mechanical properties in horizontal layers. However, as many volcanoes have complex, non-horizontal, and heterogeneous layers, we enhance these assumptions by considering mechanically diverse layers with varying dips. We employed the Finite Element Method (FEM) to create numerical models simulating two chamber shapes: a circular form and a sill-like ellipse. The primary condition was a 10 MPa excess pressure within the magma chamber, generating the stress field. Layers dips by 20-degree increments, with differing elastic moduli, represented by stiffness ratios (E_U/E_L) ranging from 0.01 to 100. Our findings validate prior research on heterogeneous crustal modeling, showing that high stiffness ratios disrupt stress within layers and induce local stress rotations at mismatched interfaces. Layer inclination further influences stress fields, shifting the location of maximum stress concentration over varying distances. This study underscores the significance of accurately understanding mechanical properties, layer dip in volcanoes, and magma chamber geometry. Improving predictions of future eruption vents in active volcanoes, particularly in the Andes with its deformed, folded, and non-horizontal stratified crust, hinges on this knowledge. By expanding stress models to incorporate complex geological structures, we enhance our ability to forecast eruption sites and the paths of magma propagation accurately.

1 Introduction

Despite progress in volcanology on the understanding of volcanic and igneous plumbing systems, there are often large uncertainties as to where a feeder-dike reaches the surface, and therefore, the location of the resulting vents or volcanic fissures (Rosi et al., 2022). This makes it difficult to assess both long and short-term hazards, which is an essential task to reduce volcanic risk (Martí et al., 2022). Eruptions can occur on or near the volcano summit, or on the flanks of cone-shaped central volcanoes, however, in volcanoes with no summit nor cone-shaped edifice, such as calderas, eruptions can occur within, around or outside the caldera, and in both cases, it is challenging to forecast where any new vent will form (Rivalta et al., 2019). Whilst it has been demonstrated that the state of stress within a volcano controls possible magma pathways (Anderson, 1951; Hutton, 1988; Rubin, 1995; Gudmundsson, 2011a; Davis et al., 2021), it is often practically challenging to measure how the stress field within a volcano varies spatially and with depth. For this reason, forward modeling techniques are required so as to estimate the level and distribution of stresses under different circumstances and boundary conditions. Available geological field data, such as past vent distributions, can also be used as markers of magma pathways. However, relying on these data is problematic as they only represent part of the total activity of a volcano or a volcanic field, they may be destroyed or buried by subsequent activity, and eruptive vents may be abandoned after a single eruption, as in monogenetic vents (Rivalta et al., 2019), and so give limited information about future vent locations. Furthermore, since the volcano stress field can be used as input for statistical analysis to predict potential vent location

(e.g., Martí and Felpeto, 2010; Schöpa et al., 2011; Cappello et al., 2012; Rivalta et al., 2019) better understanding of the factors that influence a volcanoes stress field is urgently required.

During dike injection, if, where and when the magma will reach the surface is often poorly constrained, but it is well-known that the propagation path is controlled by the crustal stress field of a volcano (Hutton, 1988; Rubin, 1995; Gudmundsson, 2011; Caricchi et al., 2021; Gudmundsson, 2022a). The stress field within a volcano is controlled partly by regional (or far-field) forces but predominantly by the form of (geometry) and pressure changes within the shallow magma chamber and the shape and size of the volcano itself (Dzurisin and Lisowski, 2007; Acocella and Neri, 2009). A further control on the distribution and magnitude of stresses relates to the properties of the rocks that constitute the volcano (e.g., Gudmundsson, 2006).

Magma-filled fractures (dikes and inclined sheets), which feed volcanic eruptions, propagate predominately in a direction oriented perpendicular to the minimum compressive (maximum tensile) principal stress σ3 and thus parallel with the maximum principal compressive stress σ3 (Anderson, 1936; Delaney et al., 1986; Rubin, 1995; Gudmundsson, 2002). Several factors may control the stress field within a volcano, such as the size, form and pressure of the underlying magma chamber or volcanic plumbing system (Gray and Monaghan, 2004; Currenti and Williams, 2014), regional forces driven by plate tectonics (e.g., Gudmundsson, 1995; Roman and Heron, 2007) or influenced by crustal faults (Lara et al., 2006; Stanton-Yonge et al., 2016, Gudmundsson, 2022a), topographic loads (e.g., Acocella and Neri, 2009; Urbani et al., 2018; Johnson et al., 2019) or unloads (e.g., Hooper et al., 2011; Gaete et al., 2019) and the, often heterogeneous and stratigraphically inclined, mechanical properties of the rocks within the volcano (Gudmundsson, 2006; Clunes et al., 2021). This last factor, essentially the local geology, either of the volcano and/or of the rocks that underlie it, have been shown to influence both the magnitude and style of intrusion-related ground deformation (Masterlark, 2007; Hickey and Gottsmann, 2014; Al Shehri and Gudmundsson, 2018; Clunes et al., 2023), but it is still not fully clear to what extent layer dip controls changes in the stress field.

In convergent margins, where the overlying crust is commonly deformed by compressional forces, such as in the Andes, crustal layers are commonly folded and faulted (Vries and Borgia, 1996). This can result in geological sequences comprising inclined layers, in some cases vertically, such as those found in the Andean fold-and-thrust belts (e.g., Kuhn, 2002; Giambiagi et al., 2003; Giambiagi et al., 2008; Sagripanti et al., 2015). This setting represents the basement architecture of many active arc volcanoes, and in turn, is reflective of the general nature of host rocks that contain intruded magmas and other fluids (Figures 1a to 1c). Magma emplacement itself may also often induces bending and deformation of host rock layers (e.g., Magee et al., 2017; Reeves et al., 2018), which will further alter the inclination of crustal layers and potential interaction with later magma injection events (Figure 1d). Inclined layers can also be found in the upper sequences of steep sided volcanic edifices with inclinations of up to 42° (Gudmundsson, 2012; Grosse et al., 2014). At depth, due to the load of the overburden, in all volcanic systems the layers become inclined, becoming dipping layers the rule (Gudmundsson, 2017). These layers are often mechanically heterogeneous, comprising intercalations of relatively compliant (low Young's

modulus) pyroclastic rocks and relatively stiff (high Young's modulus) lava flows that respond differently to the application of stress.

The combined effect of inclined and mechanically heterogeneous layers on the stress field surrounding magma chambers was first addressed by Gudmundsson (2006), who simulated a crustal segment made up of layers dipping gradually more steeply with depth. It was found that the inclination of heterogeneous layers could change both the location of stress concentrations and the orientation of the principal stresses, especially in the down-dip direction of the layers. For stress concentrations at the surface, this could imply that a dike injected from a magma chamber could reach the surface in a location shifted from that expected by assuming a non-layered crust or a crust composed by horizontal layers. However, no study has yet sought to quantify the amount of stress shift resulting from different layer inclinations and magma chamber geometries. To remedy this, we present a systematic study of the influence of rock layer dip on the distribution of crustal stresses, within a crustal segment hosting an inflating magma chamber. Here we present data from tens of Finite Element Method (FEM) models that simulate the effect of different layer inclinations and mechanical heterogeneities on the distribution of stresses around an idealized magma chamber geometry that is either circular or elliptical. We discuss our results in the context of aiding in the determination of possible dike propagation paths and the estimation of the likely location of future eruptive vents.

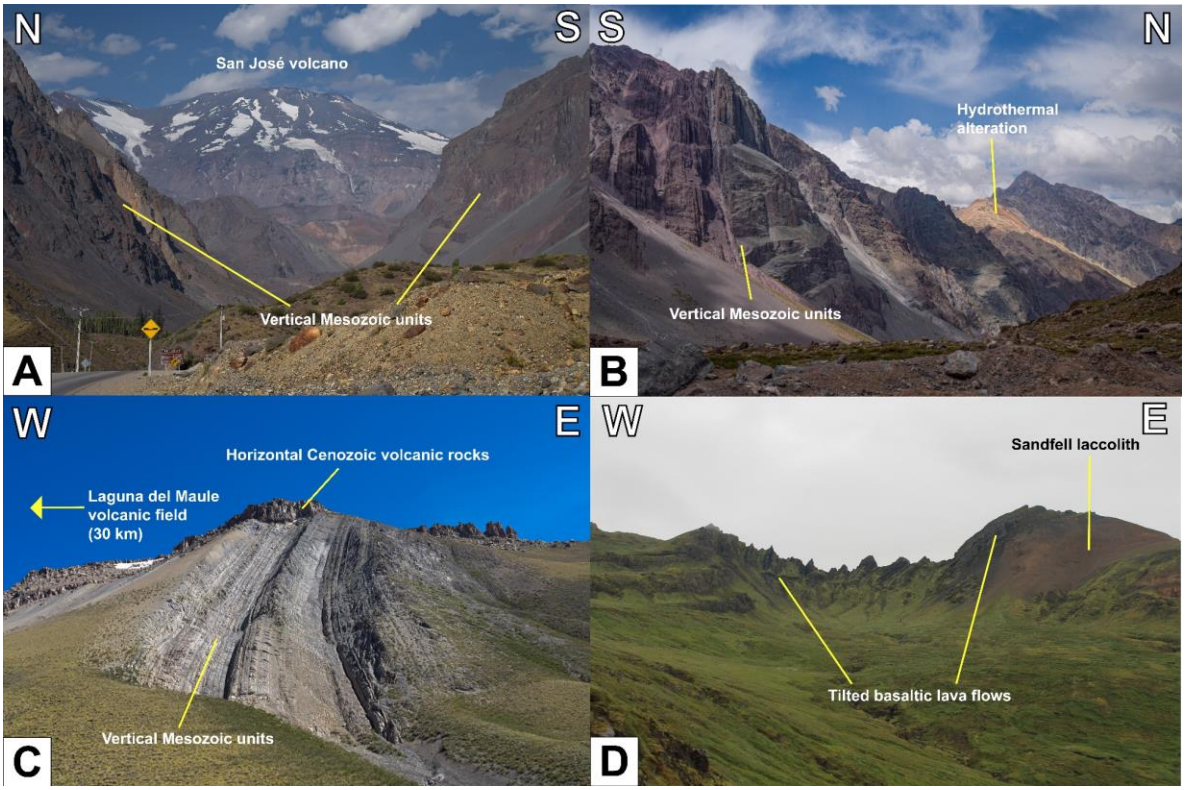

Figure 1: a. East view of the vertically layered rocks from the Lo Valdés Formation close to the active San José volcano in the western domain of the Aconcagua fold-and-thrust belt, Andes of Central Chile. b. West view of the vertically layered Lo Valdés Formation (shown in A) close to a hydrothermal alteration zone, Andes of Central Chile. c. Vertically layered rocks from the Mendoza Group, part of the Malargüe fold-and-thrust belt, located 30 km east of the Laguna del Maule volcanic field, Argentina. d. North view of the Sandfell laccolith intruding and bending the basaltic lava pile of East Iceland.

2 Methods

We use the Finite Element Method (FEM) software COMSOL Multiphysics 5.4 (https://www.comsol.com/release/5.4) to build and run two-dimensional models of an inflating (pressurized) magma chamber within a layered crustal segment where both the mechanical properties and the dips of the layers vary (Figure 2). The Structural Mechanics module in COMSOL Multiphysics solves elasticity equations to obtain stresses and displacements generated by the applied boundary conditions for each of the modeled geometries. The computational domain which represents the crustal segment is 20 km thick x 20 km width. This ensures that the chamber is located sufficiently far from the model edges so as to avoid edge effects. The upper boundary of the computational domain is defined as an initially horizontal free surface representing the Earth's crust, while the other edges of the model are fixed to avoid solid-body rotation. In all our models we implemented a triangular mesh with extremely fine mesh size across the whole domain, where the minimum element quality was in the range of 0.002566 and 0.3001 and the average element quality between 0.6121 and 0.7857.

The modeled crust is assumed to behave as a linear elastic material and is made up of between 200 to 269 layers depending on the dip of the layers that were horizontal or inclined at 10, 30, 50, 70 or 90 degrees and always 100 m thick, which is a reasonable value for volcanic rocks (Gudmundsson, 2006). The crust is modeled as mechanically heterogeneous by assigning Young's moduli values of 1, 10 and 100 GPa to the layers. The uppermost layer is represented as E_U (light grey layers in Figure 2) and the layer below as E_L (dark grey layers in Figure 2). This creates a layered sequence with alternating Young's moduli values and respective ratios (E_U/E_L) of 0.01, 0.1, 1, 10 and 100. The contacts between the layers are modeled as "mechanically strong" interfaces, which means that neither fracturing nor slip occurs along them. The Young's moduli of lava flows and tuffs have been estimated to vary widely between 128 GPa and 0.05 GPa, respectively (Gudmundsson, 2022b and references therein). Much more limited values have been proposed by Heap et al. (2020), where a typical volcanic rock mass has a Young's modulus of 5.4 GPa. The three orders of magnitude difference in Young's moduli chosen in this work, are hence perhaps larger than experimentally constrained by Heap et al. (2020) but allow us to include a wide distribution of deformation behavior hosting magma chambers in composite volcanoes such as soft sedimentary rocks and comparatively stiff intrusive rocks (Gudmundsson, 2006) as well as other crustal rocks which have undergone intense deformation (Clunes et al., 2021). For all the layers the Poisson's ratio was kept constant at 0.25 (Babiker and Gudmundsson, 2004) and the density at 2700 kg/m^3 (Glazner and Ussler, 1989).

The magma chamber was modeled as either a circular cavity or as a sill-like (elongated) cavity with an infinite in-plane extension whose center is located at the middle of the computational domain and at a depth of 3 km. The circular magma chamber has a radius of 1 km, and the top of its roof is located at a depth of 2 km. The sill-like magma chamber has a lateral dimension (width) of 4 km and a thickness of 1 km, and the top of its roof is located at a depth of 2.5 km. The depth of the centers of the cavities were kept constant so as to investigate the influence of the surrounding rock layer inclinations and mechanical contrasts, which is the main focus of the work. The

chambers were pressurized with an excess pressure of 10 MPa, which was again kept constant throughout.

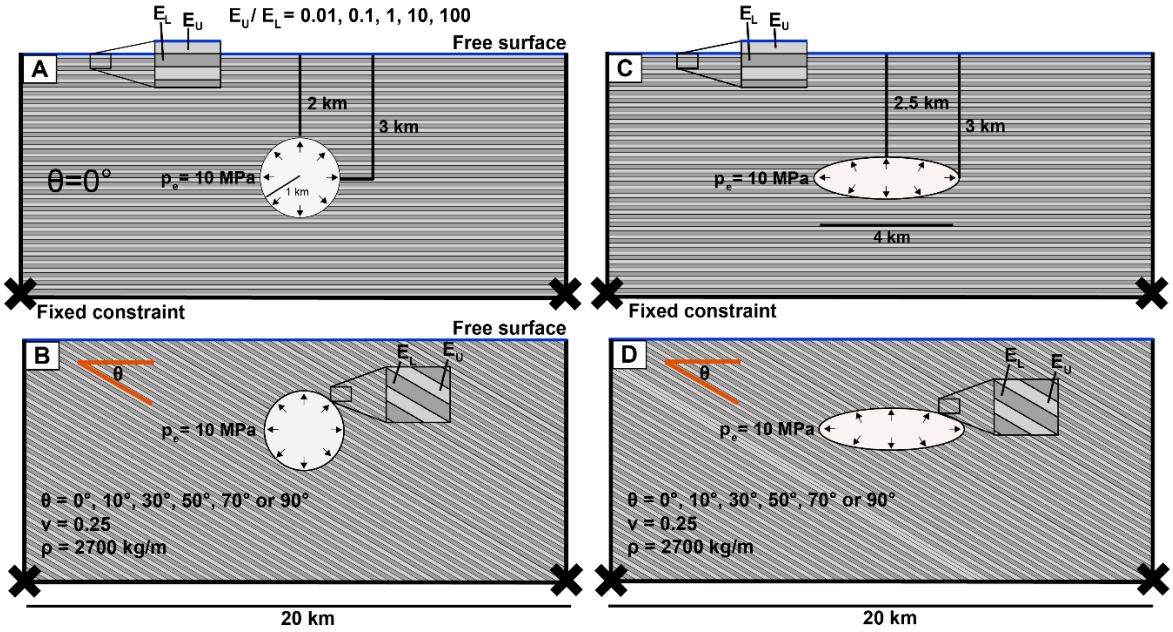

Figure 2: Finite Element Method (FEM) model setups for circular (a and b) and sill-like (c and d) inflating magma chambers represented as pressurized cavities hosted by a layered crustal segment. The different layer dip (Θ) and layer stiffness ratios tested (E_U/E_L) are shown. P_e = excess pressure; v = Poisson's ratio; ρ = rock layer density. The dimensions of the figure are not to scale. Black crosses represent the fixed edges of the computational domain, whereas the blue line along the upper edge indicates the free surface along which the resulting stresses were measured.

3. Results

The models show the distribution and magnitude of the minimum compressive (maximum tensile stress) principal stress (σ_3), and the maximum compressive principal stress (σ_1), trajectories. As normal in geology, compressive stress is regarded as positive and tensile stress as negative. Since the horizontally layered setup represents the referential state for the other setups with dipping layers, both geometries are initially within a horizontally layered crust for all the stiffness ratios tested (Figure 3 and Figure 4) are first described. Then we present the results for both chamber geometries within a crust with layers dipping at different angles tested at stiffness ratios (E_U/E_L) of 1:1, 1:10 and 1:100 (Figure 5 to Figure 10). A stiffness ratio of 1 (Figure 5 and Figure 8) represents a crust made by layers with the same Young's moduli, and the ratios of 1:10 and 1:100 highlight the effect of the mechanical layering at different layer inclinations, but only when the uppermost layer (E_U) for the horizontally layered model setup is a compliant layer, which is closer to what is expected in nature (Bazargan and Gudmundsson, 2019, 2020; Heap et al., 2020). In all cases, we first describe the results from the magma chamber modeled as a circular cavity and then as a sill-like cavity.

3.1. Horizontally layered crust

Figure 3a shows the tensile stress magnitudes induced by a pressurized circular magma chamber hosted within a horizontally layered crust measured at the top of the uppermost layer (E_U), and hence, along the free surface, and at the top of the lower layer (E_L). The maximum tensile stress is 37.5 MPa and is reached when the uppermost layer is stiff (E_U/E_L=100). When the uppermost layer (E_U) is compliant, the resulting surface tensile stresses are lower than observed when the layers have the same Young's moduli (4.7 MPa), with the lowest magnitude of 0.7 MPa obtained at at stiffness ratio (E_U/E_L) of 0.01. For all the stiffness ratios tested, the tensile stress peaks are located directly above the center of the magma chamber and the tensile stress concentrations along the free surface is symmetrically distributed around the magma chamber. Figure 3b to 3f demonstrate the minimum compressive (maximum tensile stress) principal stress concentrations (σ_3) around the pressurized circular cavity hosted by a crust composed by horizontal layers with different stiffness ratios. When the layers are horizontal, for all the stiffness ratios tested the σ_3 concentrations are symmetric around the magma chamber. When the crustal layers have the same Young's modulus (E_U/E_L=1), σ_3 concentrations are relatively homogeneously distributed around the margins of the magma chamber (Figure 3b) as expected for a non-layered crust (Figure S2a). For the other stiffness ratios σ_3 is concentrated into the stiff layers and this have an effect in how the tensile stress is distributed from the magma chamber to the surface.

Figure 4a shows the tensile stress magnitudes induced by a pressurized sill-like magma chamber hosted by a horizontally layered crust measured along the free surface for each stiffness ratio evaluated. The tensile stress induced by a sill-like chamber are higher than those induced by a circular chamber for all the stiffness ratio tested. The maximum tensile stress peak is 81.3 MPa and is reached, as the same for the circular chamber, when the uppermost layer is stiff (E_U/E_L=100). For each stiffness ratio tested, the tensile stress peak is located directly above the center of the magma chamber. In Figures 4b to 4f it is possible to note that now the tensile stress is concentrated at the margins of the sill-like chamber. The tensile stress is concentrated preferentially within the stiff layers.

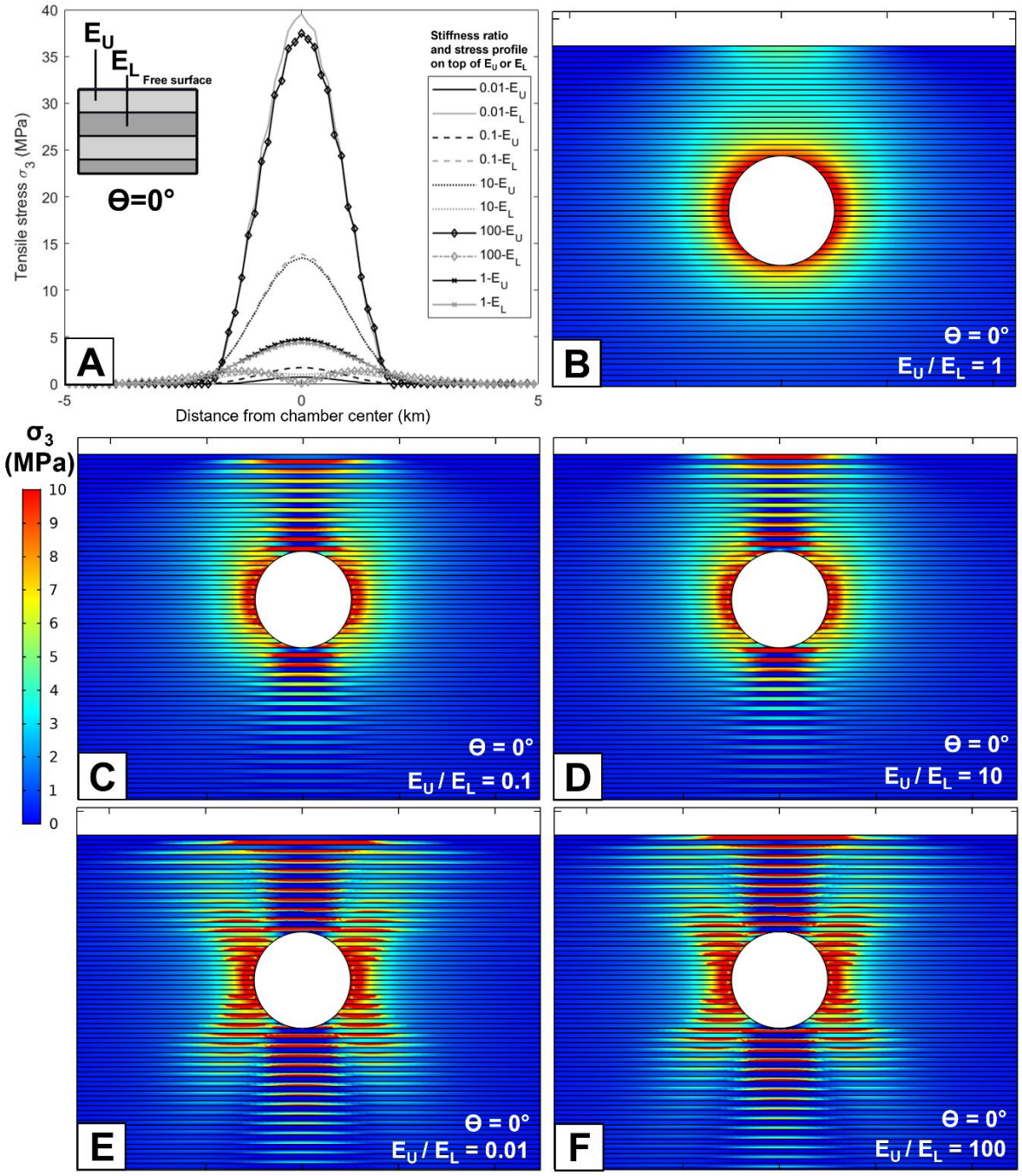

Figure 3: Model results for horizontal crustal layers and a circular inflating chamber. a. Tensile stress (σ_3) magnitudes measured atop the uppermost layer E_U (along the free surface) and atop the lower layer E_L, relative to the lateral distance from the projection of the magma chamber center over the free surface. b-f. Zoomed in section (9 km x 6 km) of Finite Element Method models of stresses around an inflating circular magma chamber hosted by a layered crust composed by 100 m thick horizontal layers (Θ=0°) with different stiffness ratios (E_U/E_L). Color contours represent the minimum compressive (maximum tensile stress) principal stress (σ_3).

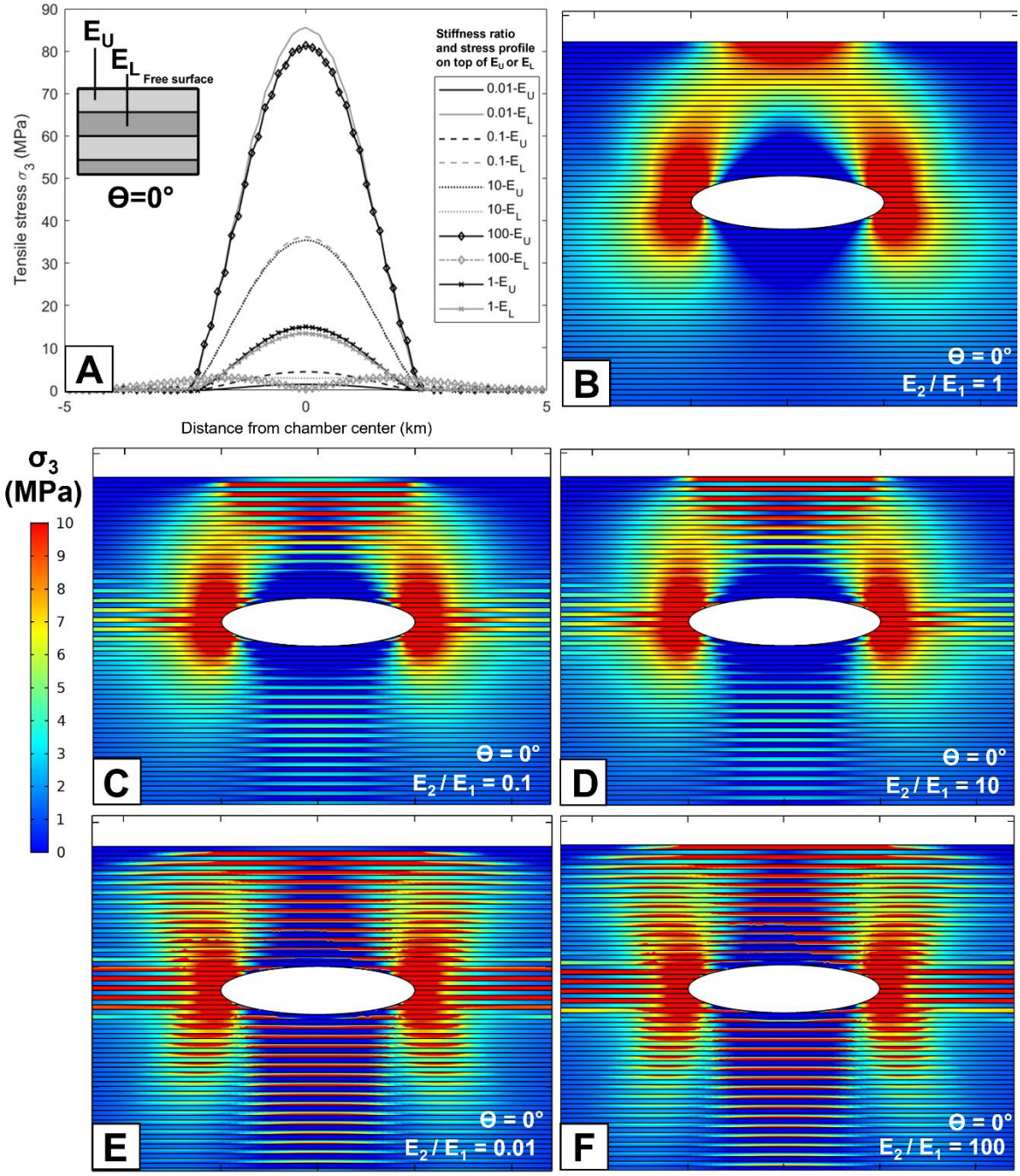

Figure 4: Model results for horizontal crustal layers and a sill-like inflating chamber. a. Tensile stress (σ_3) magnitudes measured atop the uppermost layer E_U (along the free surface) and atop the lower layer E_L, relative to the lateral distance from the projection of the sill-like magma chamber center over the free surface. b-f. Zoomed in section (9 km x 6 km) Finite Element Method models of stresses around an inflating sill-like magma chamber hosted by a layered crust composed by 100 m thick horizontal layers (Θ=0°) with different stiffness ratios (E_2/E_1). Color contours represent the minimum compressive (maximum tensile stress) principal stress (σ_3).

3.2. Crustal segment with variably dipping layers

Figure 5 shows the tensile stress concentrations (σ_3) induced by a pressurized circular magma chamber intruding a crust composed by horizontal rock layers (Figure 5a) and dipping at different angles (Figures 5b to 5f). The trajectories of the maximum compressive principal stress (σ_1) are given in Figure S2. All the modeled rock layers have the same Young's modulus of 50 GPa for all the layer inclinations tested. For all the scenarios the tensile stress concentrations and σ_1 trajectories are equally distributed around the chamber despite of the layer inclination. The tensile stress peaks of 4.7-4.8 MPa are located directly above the center of the magma chamber or with a maximum shift (Δx) of 40 m.

For the layers with a stiffness ratio (E_U/E_L) of 0.1 (Figure 6) the layer inclination affects the tensile stress concentrations both around the chamber and along the free surface. When the layers are neither horizontal nor vertical the tensile stress is distributed asymmetrically around the pressurized circular cavity. The tensile stress concentrations are shifted from above the chamber when the layers are horizontal to a position influenced by the dip of the layers. This has an effect on how the tensile stresses are distributed on surface, changing the magnitude and the location of the higher stress concentrations, which is expected to be directly above the center of the chamber for the horizontally layered model. For example, whereas the tensile stress peak of 1.7 MPa for the horizontally layered models (Figure 6a) is located at surface directly above the center of the magma chamber, the maximum tensile stress peak increases to 12.6 MPa when the layers dips by 10° (Figure 6b) and is shifted 173.3 m in the downdip direction. The maximum shifting for the stiffness ratio (E_U/E_L) of 0.1 is 660 m against the down-dip direction of the crustal segment and is generated when the layers are inclined by 50° (Figure 6d). Rotation of σ_1 does not occur for any layer inclination when the mechanical contrast between the layers is 0.1 (Figure S3).

For the layers with a stiffness ratio (E_U/E_L) of 0.01 (Figure 7) the effect of layer inclination on the location of the higher tensile stress concentrations is even more noticeable. It is again possible to observe that when the layers dips by 10° the highest tensile stress concentrations are distributed at surface but are shifted from directly above the center of the magma chamber (Figure 7b). For this scenario, the tensile stress peak is 18.1 MPa and is located 278 m in the down-dip direction. The greatest shift moves the stress peak by 1920 m against the down-dip direction and occurs when the layers are inclined by 50° (Figure 7d). For the stiffness ratio of 0.01, rotation of σ_1 occurs in a direction perpendicular to the layer inclination and at different distances from the chamber for all the layer inclinations tested (Figure S4).

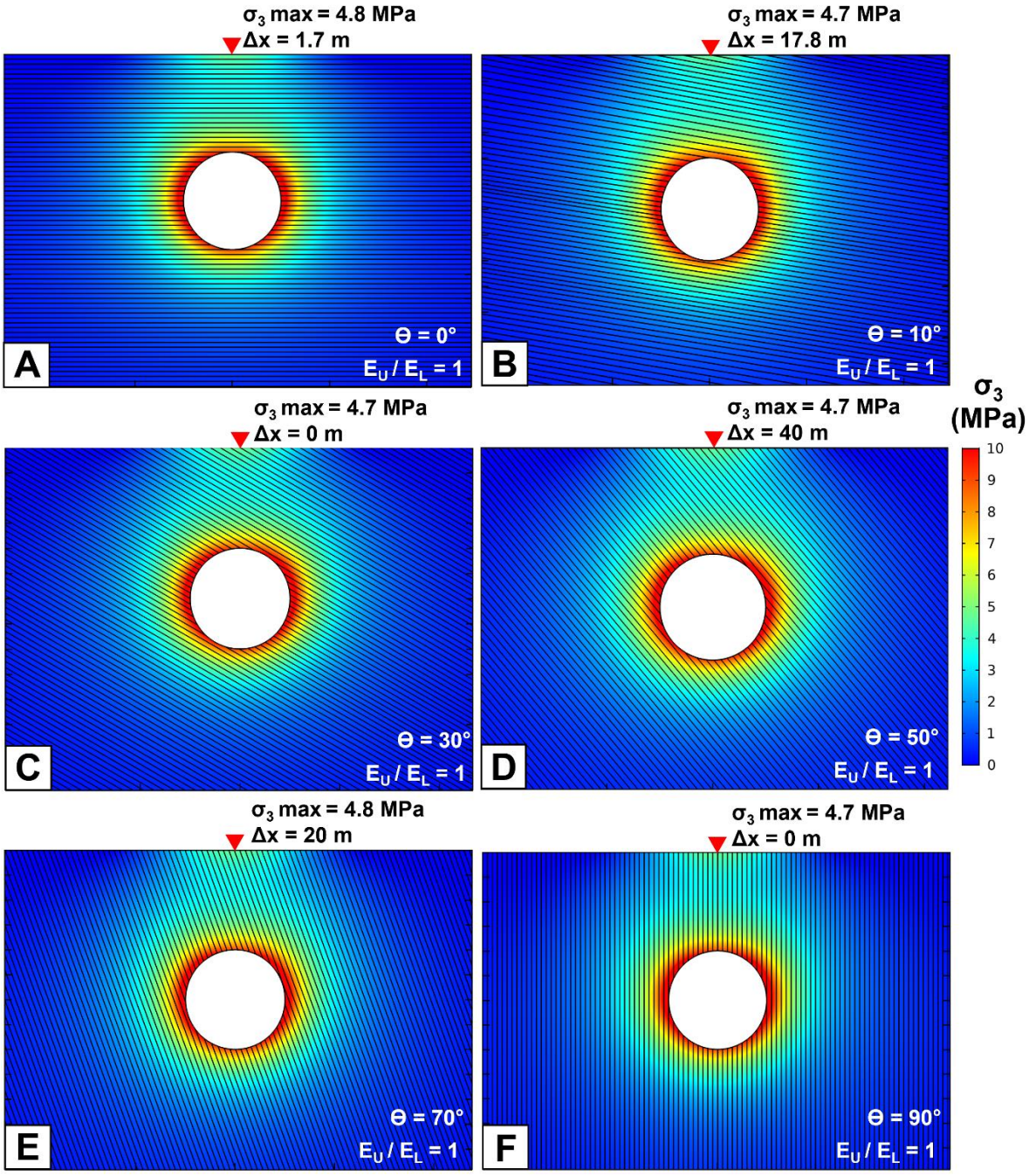

Figure 5: a-f. Finite Element Method models of stresses around a circular inflating magma chamber hosted by a layered crust composed by 100 m thick layers inclined at different angles (Θ=0°, 10°, 30°, 50°, 70° and 90°) for a stiffness ratio (E_U/E_L) of 1. Color contours represent the minimum compressive (maximum tensile stress) principal stress (σ_3). The red triangle indicates the location of the tensile stress peak at surface and the stress magnitude for each layer inclination tested.

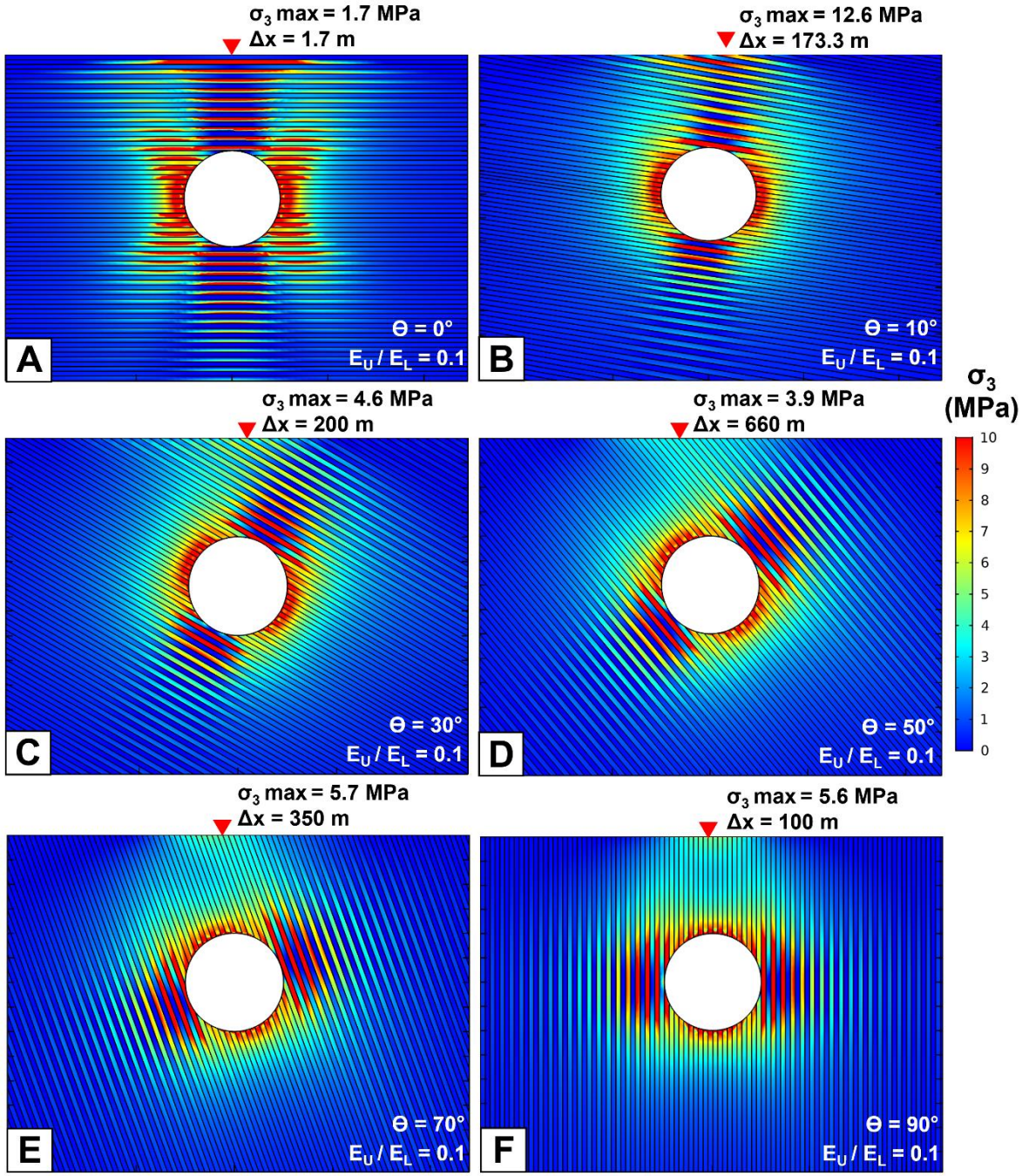

Figure 6: a-f. Finite Element Method models of stresses around a circular inflating magma chamber hosted by a layered crust composed by 100 m thick layers inclined at different angles (Θ=0°, 10°, 30°, 50°, 70° and 90°) for a stiffness ratio (E_U/E_L) of 0.1. Color contours represent the minimum compressive (maximum tensile stress) principal stress (σ_3). The red triangle indicates the location of the tensile stress peak at surface and the stress magnitude for each layer inclination tested.

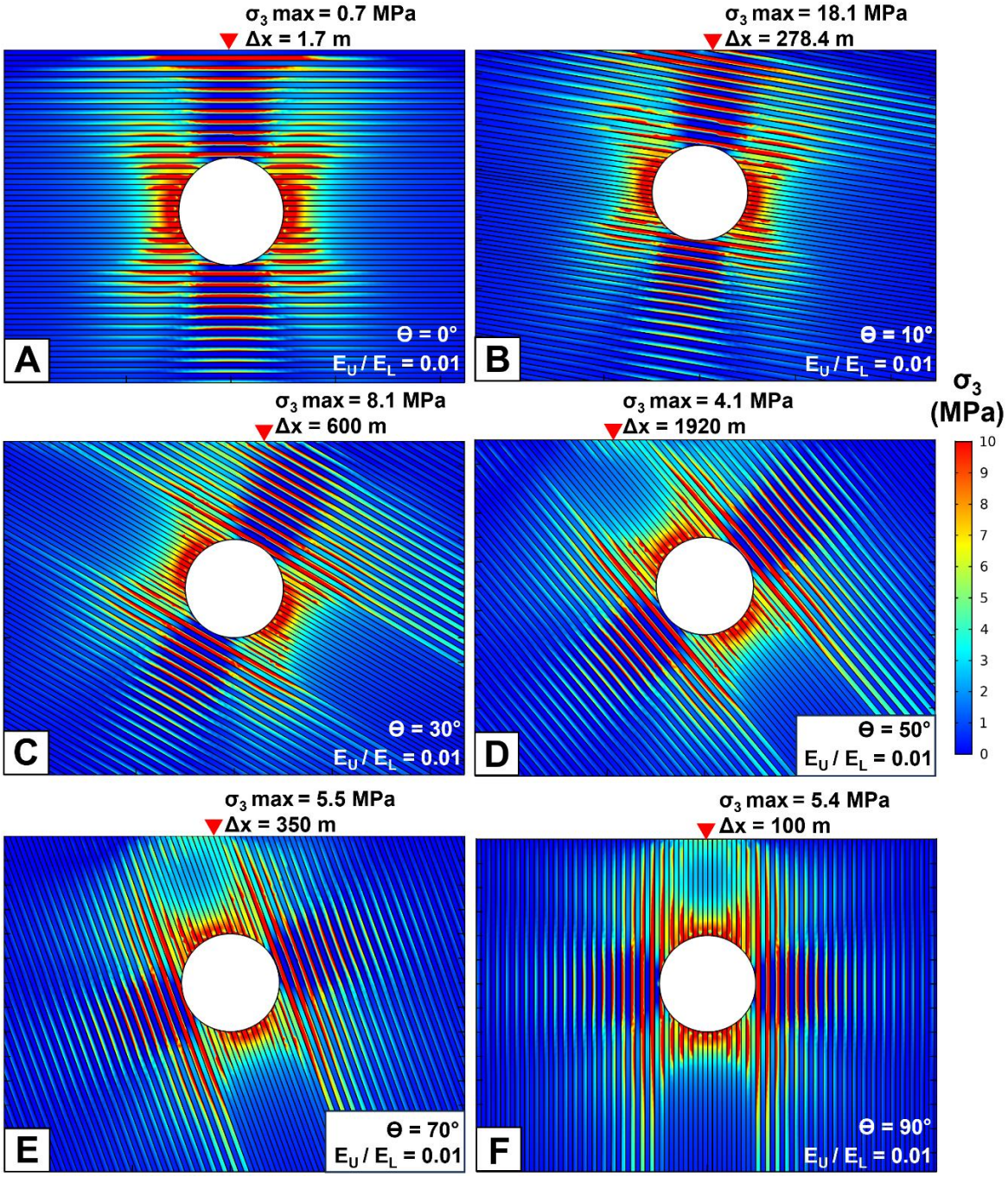

Figure 7: a-f. Finite Element Method models of stresses around a circular inflating magma chamber hosted by a layered crust composed by 100 m thick layers inclined at different angles (Θ=0°, 10°, 30°, 50°, 70° and 90°) for a stiffness ratio (E_U/E_L) of 0.01. Color contours represent the minimum compressive (maximum tensile stress) principal stress (σ_3). The red triangle indicates the location of the tensile stress peak at surface and the stress magnitude for each layer inclination tested.

As was observed for the circular magma chamber, the layer inclination has no effect on the stress distribution induced by a sill-like inflating magma chamber when the layers have the same stiffness (Figure 8). For a stiffness ratio of 1, the tensile stress is distributed symmetrically around the sill-

like chamber, preferentially concentrated at the margin of the chambers and at surface. The higher tensile stress concentrations are generated, despite the applied excess pressure remains the same (10 MPa). In this case the tensile stress peak is 14.9 MPa and is located directly above the center of the chamber or shifted by as much as 40m.

When the stiffness contrast between the layers (E_U/E_L) is 0.1(Figure 9), the tensile stress peak at surface is 4.3 MPa for the horizontally layered model and is located almost directly above the center of the sill-like chamber. The maximum tensile stress peak at surface of 32 MPa occurs when the layers dip by 10° (Figure 9b) and its location is shifted 173 m in down-dip direction of the layers, compared to what is expected for the horizontally layered model. The greatest surface tensile stress concentration shifting is generated when the layers are inclined by 30° (Figure 9c) with a distance of 400 m from what is expected for a homogeneous crust. Stress rotation develops locally and only immediately over the sill-like pressurized cavity (Figure S7).

For a mechanical contrast (E_U/E_L) of 0.01 (Figure 10) the tensile stress peak at surface is 1.4 MPa when the layers are horizontal and is located almost at the center of the computational domain (Figure 10a). The highest tensile stress concentration at surface is 40.8 MPa, located 923 m againts the down-dip direction of the layers and is generated when the layers dips by 10° (Figure 10b). The greatest tensile stress location shift (Δx) is 1220 m and occurs when the layers dips 50° (Figure 10d). Rotation of σ_1 is observed clearly at the top of compliant layers below stiff layers when the layers are horizontal (Figure S8a). For the other layer inclinations stress rotation is only locally observed and develops in a direction more or less perpendicular to the layer dip (Figure S8b to Figure S8f). This rotation occurs preferentially directly over the sill-like chamber for inclinations of 30° and greater (Figures S8c to Figure S8f) and locally between mechanically contrasting layers for an inclination of 10° (Figure S8b).

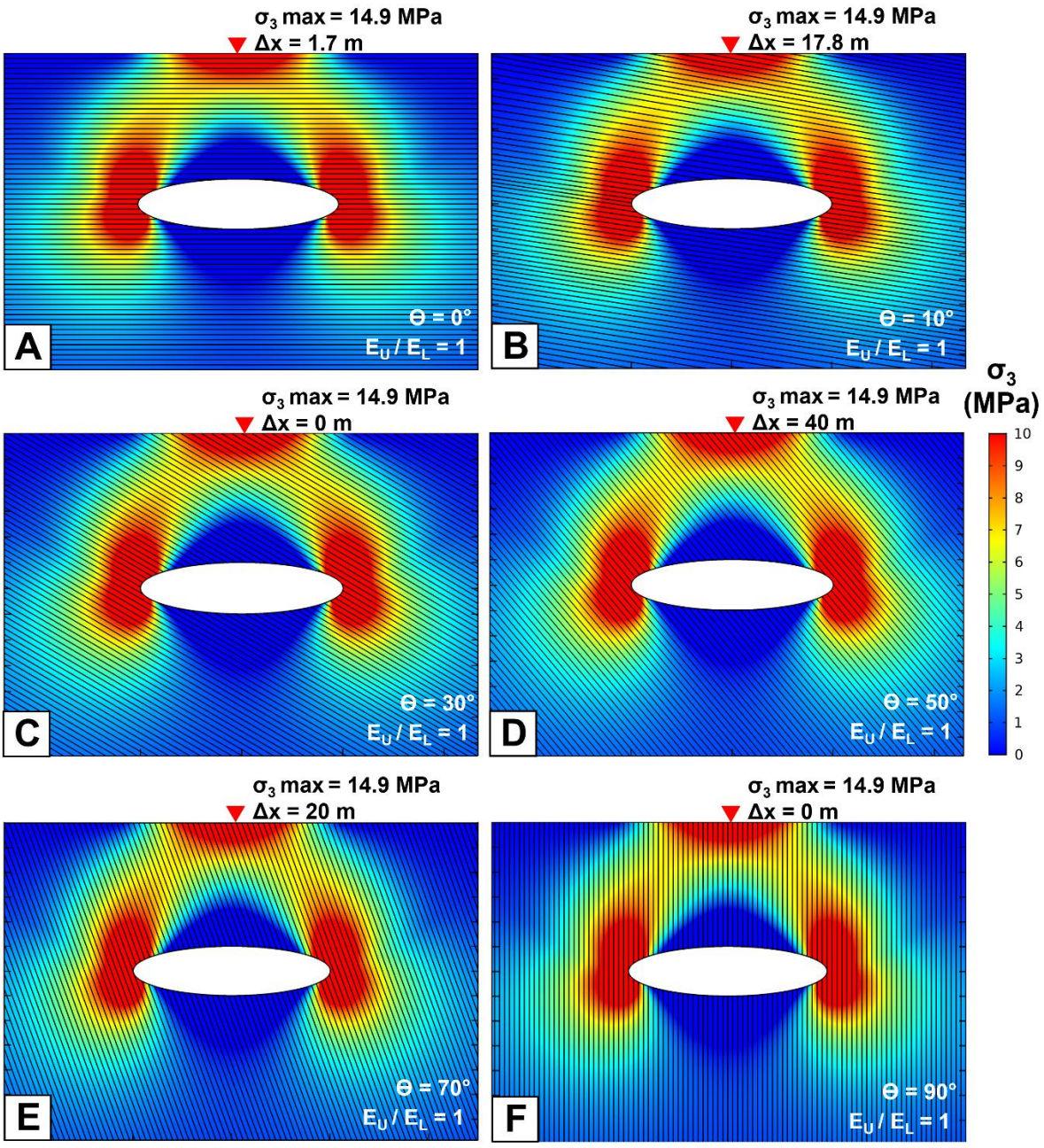

Figure 8: a-f. Finite Element Method models of stresses around a sill-like inflating magma chamber hosted by a layered crust composed by 100 m thick layers inclined at different angles (Θ=0°, 10°, 30°, 50°, 70° and 90°) for a stiffness ratio (E_U/E_L) of 1. Color contours represent the minimum compressive (maximum tensile stress) principal stress (σ_3). The red triangle indicates the location of the tensile stress peak at surface and the stress magnitude for each layer inclination tested.

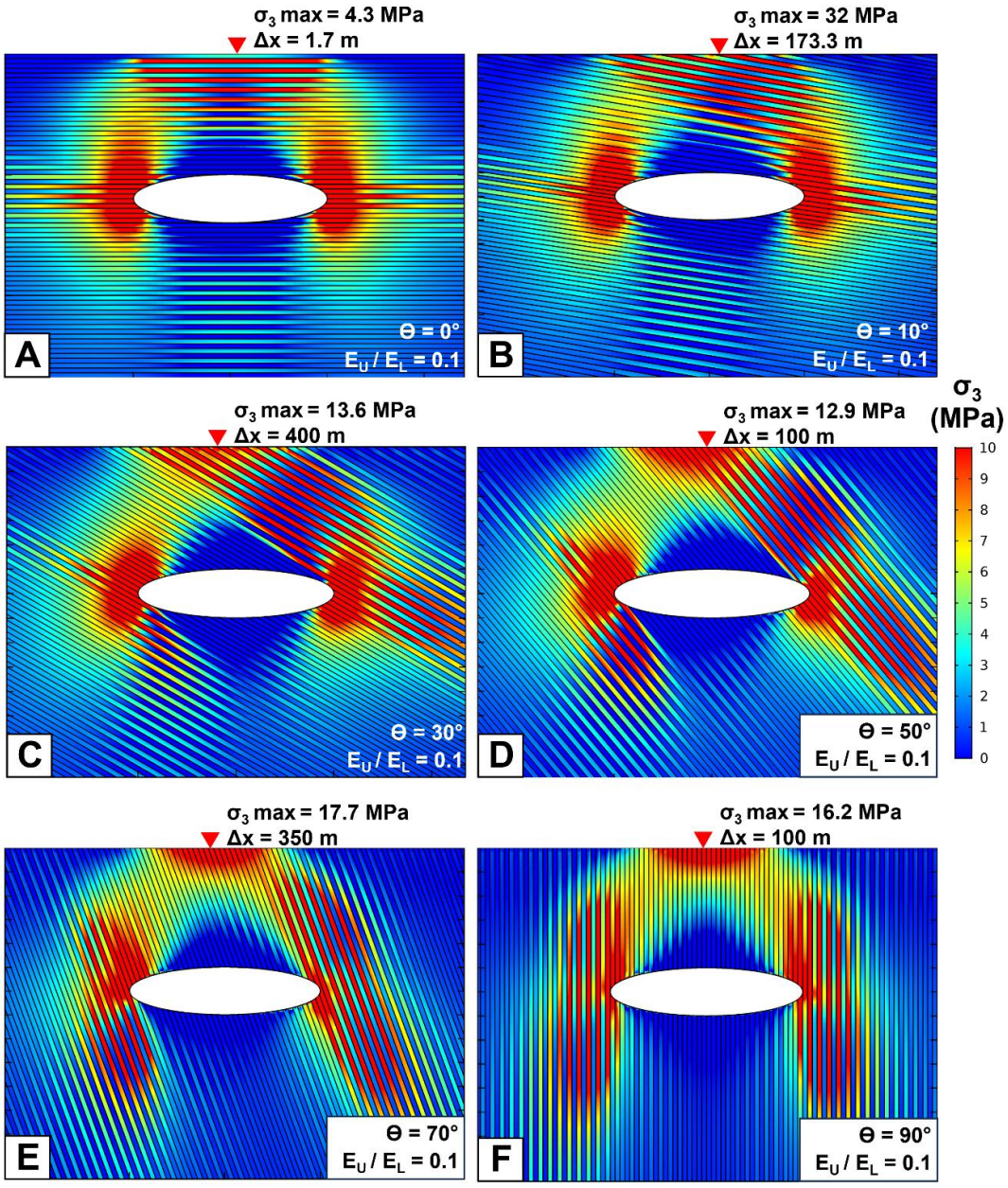

Figure 9: a-f. Finite Element Method models of stresses around an sill-like inflating magma chamber hosted by a layered crust composed by 100 m thick layers inclined at different angles (Θ=0°, 10°, 30°, 50°, 70° and 90°) for a stiffness ratio (E_U/E_L) of 0.1. Color contours represent the minimum compressive (maximum tensile stress) principal stress (σ_3). The red triangle indicates the location of the tensile stress peak at surface and the stress magnitude for each layer inclination tested.

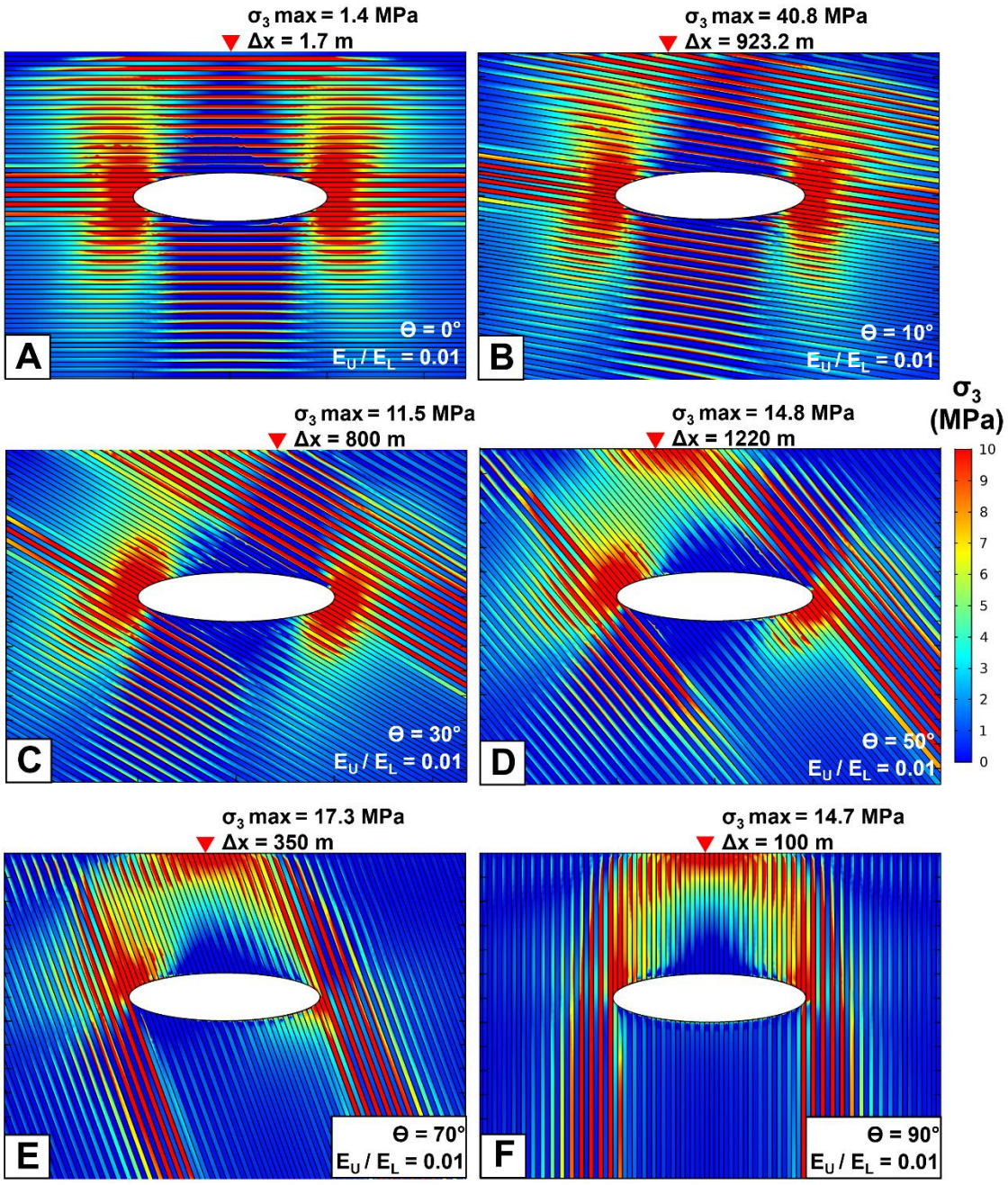

Figure 10: a-f. Finite Element Method models of stresses around a sill-like inflating magma chamber hosted by a layered crust composed by 100 m thick inclined at different angles (Θ=0°, 10°, 30°, 50°, 70° and 90°) for a stiffness ratio (E_U/E_L) of 0.01. Color contours represent the minimum compressive (maximum tensile stress) principal stress (σ_3). The red triangle indicates the location of the tensile stress peak at surface and the stress magnitude for each layer inclination tested.

4. Discussion

4.1. Mechanical layering effect on chamber-induced surface stress

Our results highlight the importance of constraining the mechanical properties of the rock layers hosting an inflating magma chamber and how the stiffness of the rocks at the surface can either show or mask stresses at depth. Depending on the surface geology above an inflating magma chamber, the induced tensile stress at surface can be significantly increased or decreased, as observed in Figures 3a and 4a, regardless of the geometry of the chamber. Despite the resulting tensile stresses presented in this work are theoretical because the in-situ tensile strength of rocks reached in nature is only up to about 9 MPa (Amadei and Stephansson, 1997), they are useful to illustrate the effect of crustal mechanical layering and layer dip. Specifically, for both circular and sill-like inflating magma chambers hosted by a horizontally layered crust, the induced tensile stress at surface is increased by almost eight times for the circular chamber and more than five times for the sill-like chamber when the uppermost rock layer (E_U) is largely stiffer than the rock layer directly beneath it (E_L), which corresponds to a stiffness ratio (E_U/E_L) of 100. (Figures S11 and S15). Conversely, when the uppermost rock layer (E_U) is largely more compliant than the rock layer directly beneath it (E_L), closer to what can be found in nature by the presence of unconsolidated deposits, which corresponds to a stiffness ratio (E_U/E_L) of 0.01, the induced tensile stress at surface is decreased by more than six times for the circular chamber and more than 10 times for the sill-like chamber. For rock layers with more similar values (i.e., E_U/E_L of 0.01 and 10) hosting circular or sill-like inflating chambers, the same observation can be made, but with more attenuated increases and decreases.

For both circular and sill-like chambers, the rotation of the maximum compressive principal stress (σ_1) is more frequent at high mechanical contrast between the layers, i.e., a stiffness ratio (E_U/E_L) of 0.01 and 100 and develops at the interface between compliant and stiff layers (Figure S4, S8, S12, S16). When this rotation of around 90° occurs in regions with high tensile stress concentration, a propagating dike could deflect into the contact between the layers and become arrested (e.g., Gudmundsson, 2002).

4.2. Effect of dipping heterogeneous rock layers on chamber-induced stresses

In Figure 11, we highlight the relationship between all the variables included in this work for pressurized circular and sill-like magma chambers, namely the magnitude of the tensile stress peak at surface, the location of the tensile stress peak in relation to the center of the chamber (Δx), the dip of the rock layers of the crustal segment hosting the chamber, and the different stiffness ratios (E_U/E_L) tested for these rock layers.. We introduce a 'stress-shift' factor (Δx) which is calculated as the distance between the location of the stress peak at surface expected for when the layers have the same Young's moduli (directly above the center of the chamber) and the location calculated for the different heterogeneous models. In Figure 11a, it is possible to note that at high layer inclinations (50, 70 and 90°) the tensile stress peaks induced by the inflating circular chamber for the different stiffness ratios tested tend to homogenize close to 5 MPa, which is the value expected fora stiffness ratio of 1. For layers dipping by 30, 10 and 0°, the effect of the mechanical contrast is prominent, especially when the layers dip by 10°. The tensile stress peak obtained for a stiffness ratio of 0.01 is 18.1 MPa, whereas for a stiffness ratio of 0.1 is 12.5 MPa, and for the stiffness contrast of 1 is 4.8 MPa in the circular magma chamber. The tensile stress peak is 40.8 MPa for a stiffness ratio of 0.01, 32 MPa for a stiffness ratio of 0.1, and 14.9 for stiffness ratio of 1, when the chamber is modeled with a sill-like geometry. When the uppermost layer (E_U) is stiff (Figure 11c) the tensile stress decreases continuously for shallow dipping layers (0-30°) and then tends to

homogenize as the dip of the layers increases. This effect highlights the importance of constraining the surface geology in volcanic regions because small changes in rock layer attitude and lithology would affect the stress field induced by magma chamber inflation, and hence, the resulting deformation signals at surface, used for eruption forecasts in volcano monitoring.

Our results show that the location of the tensile stress peak at surface is also influenced by the mechanical contrast between dipping rock layers hosting inflating magma chambers. This effect can be clearly seen in Figure 11b and 11c, where the shifting of the tensile stress peak location (Δx) relative to the location expected when the layers have the same Young's moduli is plotted against the layer dip. The largest shift of 1920 m is observed when the layers are inclined 50° and have the uppermost layer (E_U) is compliant and the stiffness contrast (E_U/E_L) is 0.01. This result is expected since at 45°, the end extent of the dipping layers is at the furthest point away from the chamber. Since a 45° layer inclination was not tested in our models, the largest shift is given at 50°. At higher layer inclinations the effect of the mechanical contrast is diminished with the tensile stress peaks at surface located close to the center of the inflating chamber. The same is observed for lower layer inclinations, but with a smaller amount of shift. The largest "stress-shift" indicates that a volcanic vent may be produced by as much as 2 km away from where would be expected assuming crustal homogeneity. In the sill-like magma chamber models the maximum "stress-shift" associated with layer inclination and heterogeneous crustal segment is less, around 1080 m, for the sill-like magma chamber than the comparative (around 2 km) for the circular chamber. This maximum shifting of the tensile stress peak occurs, as for the circular chamber, when the layers are inclined by 50°, and when the uppermost layer (E_U) is compliant and the stiffness contrast (E_U/E_L) is 0.01, but there is also an important "stress-shift" for a layer inclination of 10° (923 m), which is not observed for the circular chamber.

Despite the mechanical contrast between the layers controls the occurrence of maximum compressive principal stress (σ_1) trajectories rotation, layer inclination has an effect on the distribution of this stress rotation, which could affect where the propagating dikes could be arrested.

4.3. Magma chamber geometry

As was mentioned before, the geometry of the modeled inflating magma chamber can influence the magnitude and the distribution of resulting host rock stress field, depending on the mechanical properties of the host rock layers and the dip of these layers. When the inflating magma chamber is modeled with a sill-like geometry, the stresses tend to concentrate preferentially into the stiff layers when the crustal segment hosting the chamber is made by shallow dipping layers (Figure 11e). When the crustal segment is made by steeply dipping layers, the stresses accumulate into regions at surface (11f). It is important to note that this effect is attenuated when the magma chamber is modeled as a circular inflating chamber. This could have an effect on the distribution of fracturing and seismicity accompanying volcanic activity, and the effect of more magma chamber geometries could be tested (e.g., prolate ellipsoidal chamber, cylinder chamber).

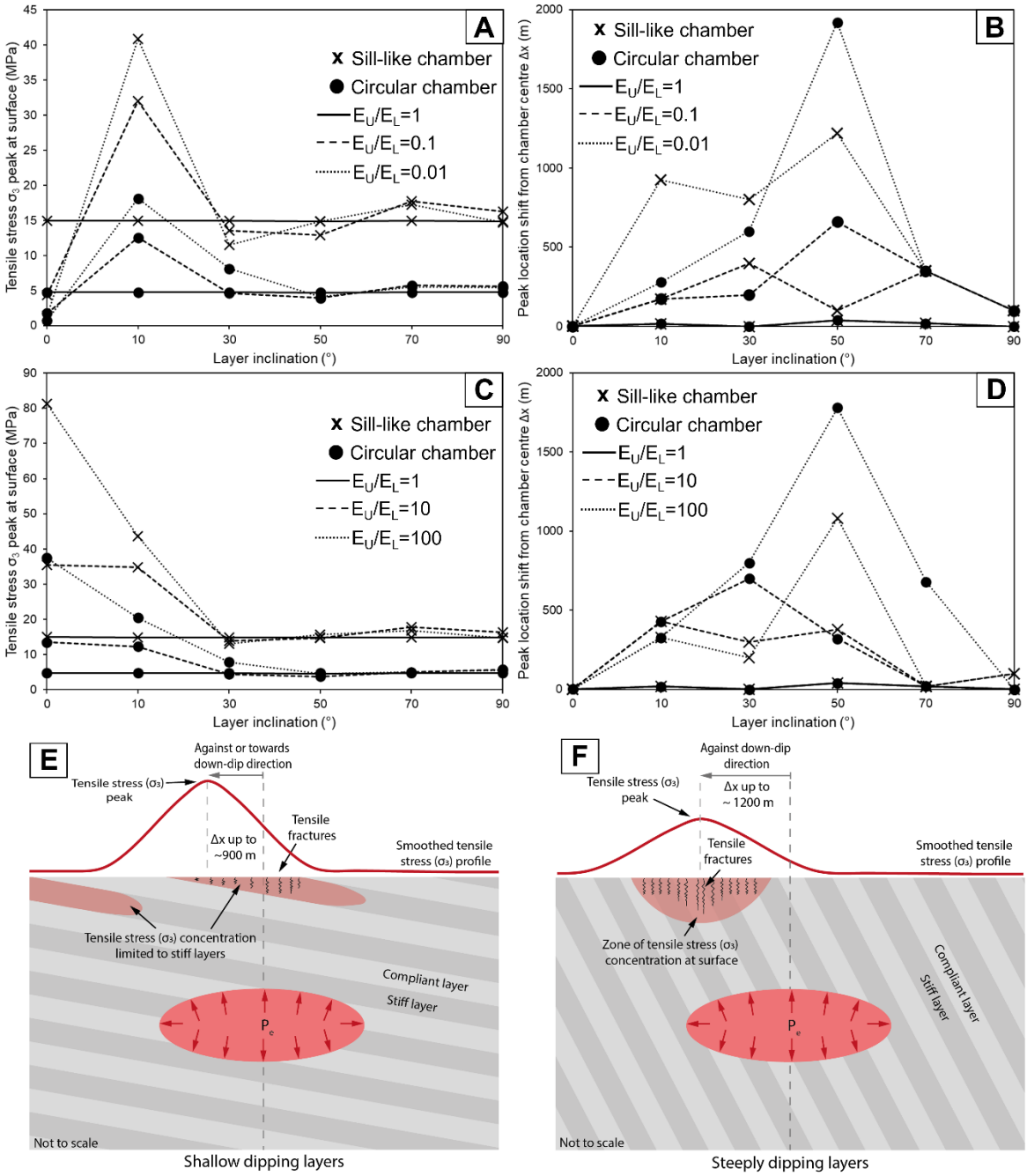

Figure 11: Comparison plots for circular (black circles) and sill-like (black crosses) inflating magma chambers for the different stiffness ratios (E_U/E_L) tested. a. Layer inclination against tensile stress peak magnitude measured at surface for stiffness ratios of 1, 0.1 and 0.01. b. Layer inclination against peak location shift from the chamber center for stiffness ratios of 1, 0,1 and 0.01. c. Layer inclination against tensile stress peak magnitude measured at surface for stiffness ratios of 1, 10 and 100. d. Layer inclination against peak location shift from the chamber center for stiffness ratios of 1, 10 and 100. e-f. Schematic illustrations showing the preferential concentration of stresses in stiff layers (e) and the formation of zones of stress accumulation (e) for a sill-like inflating magma chamber.

Taking these observations into account, conducting geological and geophysical studies to better constrain the infrastructure of volcanoes composed by mechanically heterogeneous rock layers (e.g., composite volcanoes) is relevant to the understanding of the volcano stress field (e.g., Gudmundsson, 2006; Martí and Felpeto, 2010). The scale of these studies is important, since, as was shown here and in previous studies (e.g., Bazargan and Gudmundsson, 2020) the presence of mechanical contrasts can alter considerably the tensile stress concentrations at surface, and hence, dike trajectories and the possible location of eruptive vents. Similar interpretations have been made relating to the sensitivity of magma chamber inflation induced ground deformation and the presence of compliant layers at Osmok volcano (Masterlark, 2007). We extend these results, considering variable layer dips, to suggest that areas of elevated surface stress concentration may be present and shifted by up to 2 km in either the down dip or up dip direction of the layers, in comparison to the horizontally layered case. This implies that any zone of fracturing and accompanying seismicity may also be shifted from the location expected if a homogeneous or horizontal layering is assumed. Both of these findings should be considered when monitoring volcano seismicity and surface deformation (Clunes et al., 2023). The arrangement of dipping layers, and magma chamber geometries, used in the models were not designed to represent any particular volcano but instead probe the general relation between layer dip and changes in stress field. Future models should consider deriving the precise subsurface geology of any target volcano and utilize them for forward stress modeling procedures, especially now that layer inclination is shown as a significant control.

5. Conclusions

Our results have demonstrated that mechanically heterogeneous inclined layers influence the magnitude and the location of the tensile stress induced by inflating magma chambers. Depending on the stiffness contrast between crustal rock layers hosting magma chambers and the angle of inclination of these layers, the chamber induced tensile stress can be either increased or reduced, and also shifted from the location expected when considering a non-layered crust. In the most dramatic case, with a stiffness ratio (E_U/E_L) of 0.01 and a layer inclination of 50°, the maximum level of tensile stress at the Earth's surface shifts by 1920 m when compared to a crustal segment in which the layers have the same Young's moduli for the same magma chamber form and depth. These results should be considered when attempting to forecast vent formation resulting from magma chamber rupture and dike injection.

6. Acknowledgements

This research was supported by La Agencia Nacional de Investigación y Desarrollo (ANID) through Chilean National Fund for Scientific and Technological Development (FONDECYT) projects 11190143 and 1210591 and by the Clover 2030 Open-Seed Fund. Browning further acknowledges ANID project 1220729, and Clunes acknowledges support from ANID 21202065. Kavanagh acknowledges a UK Research and Innovation (UKRI) Future Leaders Fellowship MR/S035141/1.

7. References

Acocella, V. & Neri, M. (2009). Dike propagation in volcanic edifices: overview and possible developments. *Tectonophysics*, 471(1-2), 67-77.

Al Shehri, A. & Gudmundsson, A. (2018). Modelling of surface stresses and fracturing during dyke emplacement: Application to the 2009 episode at Harrat Lunayyir, Saudi Arabia. *Journal of Volcanology and Geothermal Research*, 356, 278-303.

Amadei, B. & Stephansson, O. (1997). Rock Stress and its Measurement. Chapman and Hall, London.

Anderson, E. M. (1936). The dynamics and formation of cone-sheets, ring dikes, and cauldron-subsidence. *R. Soc. Edinb. Proc*. 128–157.

Anderson, E.M. (1951). Dynamics of Faulting and Dyke Formation. 2nd edn. Olivier and Boyd, Edinburgh.

Babiker, M. & Gudmundsson, A. (2004). The effects of dykes and faults on groundwater flow in an arid land: the Red Sea Hills, Sudan. *Journal of Hydrology*, 297(1-4), 256-273.

Bazargan, M., & Gudmundsson, A. (2019). Dike-induced stresses and displacements in layered volcanic zones. *Journal of Volcanology and Geothermal Research*, 384, 189-205.

Bazargan, M. & Gudmundsson, A. (2020). Stresses and displacements in layered rocks induced by inclined (cone) sheets: *Journal of Volcanology and Geothermal Research*, v. 401, 106965.

Caricchi, L., Townsend, M., Rivalta, E. & Namiki, A. (2021). The build-up and triggers of volcanic eruptions. *Nature Reviews Earth & Environment*, 2(7), pp.458-476.

Cappello, A., Neri, M., Acocella, V., Gallo, G., Vicari, A. & Del Negro, C. (2012). Spatial vent opening probability map of Etna volcano (Sicily, Italy). *Bulletin of Volcanology*, 74, 2083-2094.

Clunes, M., Browning, J., Cembrano, J., Marquardt, C. & Gudmundsson, A. (2021). Crustal folds alter local stress fields as demonstrated by magma sheet—fold interactions in the Central Andes. *Earth and Planetary Science Letters*, 570, 117080.

Clunes, M., Browning, J., Marquardt, C., Cortez, J., Drymoni, K. & Kavanagh, J. (2023). Inclination and heterogeneity of layered geological sequences influence dike-induced ground deformation. *Geology*, 51(3), 278-283.

Currenti, G. & Williams, C.A. (2014). Numerical modeling of deformation and stress fields around a magma chamber: Constraints on failure conditions and rheology. *Physics of the Earth and Planetary Interiors*, 226, pp.14-27.

Davis, T., Bagnardi, M., Lundgren, P. & Rivalta, E., (2021. Extreme curvature of shallow magma pathways controlled by competing stresses: insights from the 2018 Sierra Negra eruption. *Geophysical Research Letters*, 48(13), p.e2021GL093038.

Delaney, P.T., Pollard, D.D., Ziony, J.I. & McKee, E.H. (1986). Field relations between dikes and joints: emplacement processes and paleostress analysis. *J. Geophys. Res., Solid Earth* 91 (B5), 4920–4938.

Dzurisin, D. & Lisowski, M. (2007). Analytical volcano deformation source models. Volcano deformation: *Geodetic monitoring techniques*, 279-304.

Gaete, A., Kavanagh, J. L., Rivalta, E., Hazim, S. H., Walter, T. R. & Dennis, D. J.(2019). The impact of unloading stresses on post-caldera magma intrusions. *Earth and Planetary Science Letters*, 508, 109-121.

Giambiagi, L. B., Alvarez, P. P., Godoy, E., & Ramos, V. A. (2003). The control of pre-existing extensional structures on the evolution of the southern sector of the Aconcagua fold and thrust belt, southern Andes. *Tectonophysics*, 369(1-2), 1-19.

Giambiagi, L., Bechis, F., García, V., & Clark, A. H. (2008). Temporal and spatial relationships of thick-and thin-skinned deformation: A case study from the Malargüe fold-and-thrust belt, southern Central Andes. *Tectonophysics*, 459(1-4), 123-139.

Glazner, A. F. & Ussler III, W. (1989). Crustal extension, crustal density, and the evolution of Cenozoic magmatism in the Basin and Range of the western United States. *Journal of Geophysical Research: Solid Earth*, 94(B6), 7952-7960.

Gray, J.P. & Monaghan, J.J. (2004). Numerical modelling of stress fields and fracture around magma chambers. *Journal of Volcanology and Geothermal Research*, 135(3), pp.259-283.

Grosse, P., Euillades, P. A., Euillades, L. D., & Van Wyk de Vries, B. (2014). A global database of composite volcano morphometry. *Bulletin of Volcanology*, 76, 1-16.

Gudmundsson, A. (1995). Infrastructure and mechanics of volcanic systems in Iceland. *Journal of Volcanology and Geothermal Research*, 64(1-2), 1-22.

Gudmundsson, A. (2002). Emplacement and arrest of sheets and dykes in central volcanoes. *Journal of Volcanology and Geothermal Research*, 116, 279-298.

Gudmundsson, A. (2006). How local stresses control magma-chamber ruptures, dyke injections, and eruptions in composite volcanoes. *Earth-science reviews*, 79(1-2), 1-31.

Gudmundsson, A. (2011). Deflection of dykes into sills at discontinuities and magma-chamber formation. *Tectonophysics*, 500(1-4), 50-64.

Gudmundsson, A. (2012). Strengths and strain energies of volcanic edifices: Implications for eruptions, collapse calderas, and landslides: *Natural Hazards and Earth System Sciences*, v. 12, p. 2241–2258.

Gudmundsson, A. (2017). The glorious geology of Iceland's golden circle (p. 334). Cham, Switzerland: *Springer International Publishing.*

Gudmundsson, A. (2022a). The propagation paths of fluid-driven fractures in layered and faulted rocks. *Geological Magazine*, 159(11-12), 1978-2001.

Gudmundsson, A. (2022b). Volcanotectonics. Understanding the Structure, Deformation and Dynamics of Volcanoes. Cambridge University Press.

Heap, M. J., Villeneuve, M., Albino, F., Farquharson, J. I., Brothelande, E., Amelung, F., Got, J. L. & Baud, P. (2020). Towards more realistic values of elastic moduli for volcano modelling. *Journal of Volcanology and Geothermal Research*, 390, 106684.

Hickey, J., & Gottsmann, J. (2014). Benchmarking and developing numerical Finite Element models of volcanic deformation. *Journal of Volcanology and Geothermal Research*, 280, 126-130.

Hooper, A., Ófeigsson, B., Sigmundsson, F., Lund, B., Einarsson, P., Geirsson, H. & Sturkell, E. (2011). Increased capture of magma in the crust promoted by ice-cap retreat in Iceland. Nature *Geoscience*, 4(11), 783-786.

Hutton, D. H. (1988). Granite emplacement mechanisms and tectonic controls: inferences from deformation studies. *Earth and Environmental Science Transactions of the Royal Society of Edinburgh*, 79(2-3), 245-255.

Johnson, J. H., Poland, M. P., Anderson, K. R. & Biggs, J. (2019). A cautionary tale of topography and tilt from Kīlauea Caldera. *Geophysical Research Letters*, 46(8), 4221-4229.

Kuhn, D. (2002). Fold and thrust belt structures and strike-slip faulting at the SE margin of the Salar de Atacama basin, Chilean Andes. *Tectonics*, 21(4), 8-1.

Lara, L.E., Lavenu, A., Cembrano, J. & Rodríguez, C. (2006). Structural controls of volcanism in transversal chains: resheared faults and neotectonics in the Cordón Caulle–Puyehue area (40.5 S), Southern Andes. *Journal of Volcanology and Geothermal Research*, *158*(1-2), pp.70-86.

Magee, C., Bastow, I. D., de Vries, B. V. W., Jackson, C. A. L., Hetherington, R., Hagos, M. & Hoggett, M. (2017). Structure and dynamics of surface uplift induced by incremental sill emplacement. *Geology*, 45(5), 431-434.

Marti, J. & Felpeto, A. (2010). Methodology for the computation of volcanic susceptibility: an example for mafic and felsic eruptions on Tenerife (Canary Islands). *Journal of Volcanology and Geothermal Research*, 195(1), 69-77.

Martí, J., Becerril, L. & Rodríguez, A. (2022). How long-term hazard assessment may help to anticipate volcanic eruptions: The case of La Palma eruption 2021 (Canary Islands). *Journal of Volcanology and Geothermal Research*, 431, 107669.

Masterlark, T. (2007). Magma intrusion and deformation predictions: sensitivities to the Mogi assumptions. *J. Geophys. Res., Solid Earth*112 (B6).

Reeves, J., Magee, C. & Jackson, C.A.L. (2018). Unravelling intrusion-induced forced fold kinematics and ground deformation using 3D seismic reflection data. *Volcanica*, 1(1), pp.1-17.

Rivalta, E., Corbi, F., Passarelli, L., Acocella, V., Davis, T., Di Vito, M. A. 2019. Stress inversions to forecast magma pathways and eruptive vent location. *Science advances*, 5(7).

Roman, D.C. & Heron, P. (2007). Effect of regional tectonic setting on local fault response to episodes of volcanic activity. Geophysical Research Letters, 34(13).

Rosi, M., Acocella, V., Cioni, R., Bianco, F., Costa, A., De Martino, P., Giordano, G. & Inguaggiato, S. (2022). Defining the pre-eruptive states of active volcanoes for improving eruption forecasting. *Frontiers in Earth Science*, 10, p.795700.

Rubin, A. M. (1995). Propagation of magma-filled cracks. *Annual Review of Earth and Planetary Sciences*, 23(1), 287-336.

Sagripanti, L., Vera, E. A. R., Gianni, G. M., Folguera, A., Harvey, J. E., Farías, M., & Ramos, V. A. (2015). Neotectonic reactivation of the western section of the Malargüe fold and thrust belt (Tromen volcanic plateau, Southern Central Andes). *Geomorphology*, 232, 164-181.

Schöpa, A., Pantaleo, M. & Walter, T. R. (2011). Scale-dependent location of hydrothermal vents: Stress field models and infrared field observations on the Fossa Cone, Vulcano Island, Italy. *Journal of Volcanology and Geothermal Research*, 203(3-4), 133-145.

Stanton-Yonge, A., Griffith, W.A., Cembrano, J., St. Julien, R. & Iturrieta, P. (2016). Tectonic role of margin-parallel and margin-transverse faults during oblique subduction in the Southern Volcanic Zone of the Andes: Insights from Boundary Element Modeling. *Tectonics*, *35*(9), pp.1990-2013.

Urbani, S., Acocella, V. & Rivalta, E. (2018). What drives the lateral versus vertical propagation of dikes? Insights from analogue models. *Journal of Geophysical Research: Solid Earth*, 123(5), 3680-3697.

van Wyk de Vries, B. & Borgia, A. (1996). The role of basement in volcano deformation. *Geological Society*, London, Special Publications, 110(1), pp.95-110.